Nanostructured SERS-electrochemical biosensors for testing of anticancer drug interactions with DNA

Hoda Ilkhani, Taylor Hughes, Jing Li, Chuan Jian Zhong, Maria Hepel

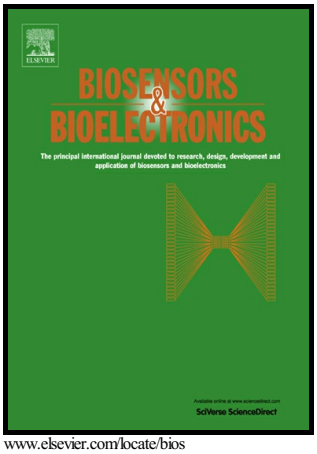

www.elsevier.com/locate/bios

PII: S0956-5663(16)30077-X
DOI: http://dx.doi.org/10.1016/j.bios.2016.01.068
Reference: BIOS8408

To appear in: *Biosensors and Bioelectronic*

Received date: 13 December 2015
Revised date: 26 January 2016
Accepted date: 28 January 2016

Cite this article as: Hoda Ilkhani, Taylor Hughes, Jing Li, Chuan Jian Zhong and Maria Hepel, Nanostructured SERS-electrochemical biosensors for testing of anticancer drug interactions with DNA, *Biosensors and Bioelectronic* http://dx.doi.org/10.1016/j.bios.2016.01.068

Nanostructured SERS-electrochemical biosensors for testing of anticancer drug interactions with DNA

Hoda Ilkhani[1], Taylor Hughes[1], Jing Li[2], Chuan Jian Zhong[2], and Maria Hepel[1]*

[1]*Department of Chemistry, State University of New York at Potsdam, Potsdam, NY 13676, USA*
[2]*Department of Chemistry, State University of New York at Binghamton, Binghamton, NY 13902,USA*

* Corresponding Author address:

Professor Maria Hepel

Department of Chemistry, State University of New York at Potsdam, Stowell Hall 302,

44 Pierrepont Ave., Potsdam, NY 13676, USA

Phone: +1.315.267.2267

Fax: +1.315.267.3170

Website: www2.potsdam.edu/hepelmr

E-mail: hepelmr@potsdam.edu

Abstract

Widely used anti-cancer treatments involving chemotherapeutic drugs result in cancer cell damage due to their strong interaction with DNA. In this work, we have developed laboratory biosensors for screening chemotherapeutic drugs and to aid in the assessment of DNA modification/damage caused by these drugs. The sensors utilize surface-enhanced Raman scattering (SERS) spectroscopy and electrochemical methods to monitor sensory film modification and observe the drug-DNA reactivity. The self-assembled monolayer protected gold-disk electrode (AuDE) was coated with a reduced graphene oxide (rGO), decorated with plasmonic gold-coated Fe_2Ni@Au magnetic nanoparticles functionalized with double-stranded DNA (dsDNA), a sequence of the breast cancer gene BRCA1. The nanobiosensors AuDE/SAM/rGO/Fe_2Ni@Au/dsDNA were then subjected to the action of a model chemotherapeutic drug, doxorubicin (DOX), to assess the DNA modification and its dose dependence. The designed novel nanobiosensors offer SERS/electrochemical transduction, enabling chemically specific and highly sensitive analytical signals generation. The SERS measurements have corroborated the DOX intercalation into the DNA duplex whereas the electrochemical scans have indicated that the DNA modification by DOX proceeds in a concentration dependent manner, with limit of detection LOD = 8 μg/mL (S/N = 3), with semilog linearity over 3 orders of magnitude. These new biosensors are sensitive to agents that interact with DNA and facilitate the analysis of functional groups for determination of the binding mode. The proposed nanobiosensors can be applied in the first stage of the drug development for testing the interactions of new drugs with DNA before the drug efficacy can be assessed in more expensive testing *in vitro* and *in vivo*.

Keywords: SERS/electrochemical biosensor; breast cancer; doxorubicin; chemotherapeutic drug screening; DNA biosensor; genosensor.

1. Introduction

Extensive investigations have recently been carried out to develop new anti-cancer drugs for treatment of this widespread disease killing millions of people annually. Chemotherapy, photodynamic therapy, and hyperthermic therapy remain some of the most widely applied treatments (Burgess 2012; Du et al. 2015; Yang et al. 2015). Particular attention in studies of new anticancer drugs has been paid to increase the drug efficacy toward killing cancer cells while limiting their devastating effects on healthy cells through the targeted approach based on cancer cell biorecognition strategy (Holohan et al. 2013; Tacar et al. 2013). In this work, we have focused on the development of a laboratory nanobiosensor for screening of anticancer drugs. The sensor utilizes surface-enhanced Raman scattering (SERS) spectroscopy and electrochemical relaxation techniques, enabling the assessment of anticancer drug interactions with DNA bound to the nanostructured SERS/electrochemical biosensor surface. While SERS biosensors have been extensively investigated owing to their high sensitivity and chemical identification capabilities (see excellent reviews: (Baia 2012; Bantz et al. 2011; Huh et al. 2009)), the SERS studies of drug interactions with DNA have been scarce (Beljebbar et al. 1995; Lee et al. 2004; Li et al. 2015; Stanicová et al. 1999) and we have not found any reports on nanostructured SERS/electrochemical biosensors designed specifically for that purpose. Perspective analytical applications of novel SERS nanostructures have recently been reviewed (Li et al. 2015; Tokonami et al. 2012; Tripp et al. 2008).

The detection of DNA damage is the key challenge in studies of mutations, carcinogenesis, and aging (Hepel et al. 2012b). The use of the sophisticated instrumentation necessary for DNA analysis, such as the mass spectrometry, poses a problem in small labs around the world due to the high cost and the requirement of highly qualified personnel. This problem is effectively addressed by the new wave of nanobiosensors which can provide high sensitivity, low detection limit, and ease of use to these measurements. Thus, the DNA biosensors became an important tool in cancer diagnostics and DNA detection (Hepel et al. 2012b; Lu et al. 2013; Wei et al. 2014a).

Among different strategies utilized in designing genosensors, the electrochemical and spectroscopic methods of signal transduction have been the most attractive ones because of their high sensitivity and selectivity (Wei et al. 2014a). The detection of cancer biomarkers using

voltammetric methods offers fast and convenient analysis (Chikkaveeraiah et al. 2012; Labib et al. 2013). Highly sensitive genosensors for detection of mutations of breast cancer gene BRCA1 have recently been designed (Benvidi et al. 2015) and tested using electrochemical impedance spectroscopy, differential pulse voltammetry, and cyclic voltammetry. High sensitivity toward the interaction of dsDNA of BRCA1 with estrogen receptor alpha (ERα) controlling the gene expression has been achieved using biosensors based on silicon nanowires, acting as the field-effect transistors (Zhang et al. 2011a).

On the other hand, the surface-enhanced Raman scattering (SERS) spectroscopy, which can distinguish nucleobases and DNA (Lierop et al. 2011; Lim and al. 2011; Liu et al. 2011; Ye et al. 2012; Zhang et al. 2011c) has recently been applied to detect cancer biomarkers (Li et al. 2013; Panikkanvalappil et al. 2013; Samanta et al. 2011; Tabakman et al. 2011), including carcinoembryonic antigen (Chon et al. 2009; Tabakman et al. 2011), immunoglobulin G protein (Li et al. 2013), MUC4 (Wang and al. 2011a), and others. Noninvasive blood plasma or whole blood tests using SERS sensors have been demonstrated for several cancers, including nasopharyngeal (Lin et al. 2014), gastric (Feng and al. 2011), cervical (Feng and al. 2013), lung (Chon et al. 2009), head and neck (Wang and al. 2011b), breast (Sha and al. 2008), and other cancers. Magnetic beads coated with anti-epithelial cell adhesion molecules (EpCAM) have been applied to isolate circulating tumor cells (CTC) enabling highly sensitive SERS detection of breast cancer cells (Sha and al. 2008) and squamous cell carcinoma of head and neck (Wang and al. 2011b). Recently, autonomous DNA systems have been advised for amplified SERS detection of cancer cells based on aptamer cell recognition (Ye et al. 2012). SERS detection of cells was also investigated by other groups (Lee et al. 2011; Sha et al. 2008). Studies of the anticancer drugs and their interactions with DNA have been reported for a number of drugs, including anthracycline antitumor antibiotics, daunorubicin and doxorubicin (Beljebbar et al. 1995; Eliasson et al. 2001; Fodor et al. 1985; Gautier et al. 2013; Lee et al. 2004; Miskovsky et al. 1995; Nabiev et al. 1991; Prescott et al. 1984; Stanicová et al. 1999) using either Raman spectroscopy or SERS with silver colloid plasmonic enhancer.

While the detection of DNA using specially designed biosensors has been accomplished and utilized in a variety of practical assays, the studies of DNA damage processes using biosensors have been rare. In our earlier work (Hepel et al. 2012b), we have studied the oxidation of guanine to 8-hydroxy-guanine and DNA strand braking caused by hydroxyl radicals and

superoxide anion radicals $O_2^{\bullet-}$ generated in Fenton-type reaction of catechol in the presence of Cu(II) ions. Likewise, the damage of DNA strands immobilized on a biosensor surface by a range of common pesticides have been investigated using a DNA biosensor with electrochemical monitoring of the intercalation activity of a redox probe (Hepel and Stobiecka 2010, 2011; Hepel et al. 2012a; Nowicka et al. 2010). The oxidative damage to DNA by adriamycin has been investigated by Oliveira-Brett et al. using electrochemical techniques (Oliveira-Brett et al. 2002). Labuda and coworkers designed a nanostructured electrochemical DNA biosensor for studies of the effect of berberine and quinazolines on cancer cell DNA (Galandová et al. 2009; Ovádeková et al. 2006) and Braunhut et al. studied the effect of taxane treatment of human breast cancer cells using quartz crystal nanobalance (Brauhut et al. 2005). The detection of DNA damage by reactive nitrogen species (Zhang et al. 2012), hydroquinone (Tang et al. 2014), xanthine oxidase-induced ROS (Xiong et al. 2013) and Cd(II) ions (Zhang et al. 2011b) have also been reported. An electrochemical assay for DNA damage enabled detection of damage by styrene oxide, $NaAsO_2$, Cu(II)/H_2O_2 and UV radiation (Wei et al. 2014b). The DNA damage caused by visible light-induced ROS on mesoporous TiO_2 particles surface on a FTO/TiO_2/dopamine/DNA biosensor has been detected using square-wave voltammetry (Imani et al. 2014). Hence, these studies show clearly that the investigations of DNA interactions with active compounds using DNA biosensors are feasible and when combined with chemical identification capabilities of Raman spectroscopy in a SERS/electrochemical transduction, they could offer a viable alternative to other sensing platforms.

Therefore, in this work, we have developed a new nanostructured SERS-electrochemical biosensor, designed for screening and investigations of anticancer drugs to provide the assessment of the drug ability to intercalate and/or damage DNA molecules. For the first time, we have investigated the intercalation of a common chemotherapeutic drug doxorubicin (DOX) to breast cancer DNA, immobilized on a nanostructured biosensor surface.

The sensor developed in this work was designed for screening new drugs and their effects on DNA samples. Since this type of work requires thousands of potential drugs to be tested, the method relies on simple, reproducible standard DNA samples attached to the sensor surface instead of expensive, hard to maintain and standardize real biological samples containing vast amounts of proteins, cell debris, and various active biocompounds.

2. Materials and methods

2..1. Materials

All chemicals used were of analytical grade purity. The anticancer drug, doxorubicin (DOX), was received from Sigma-Aldrich Chemical Company (St Louis, MO, U.S.A.) and used as received. The tiols: 1,6-hexanedithiol (HDT), 1-octanethiol (OT), cysteamine (CYS), mercaptohexanol (MCH), mercaptobenzoic acid (MBA), and 3,6 dioxa-1,8-octane dithiol (DODT) were obtained from Sigma-Aldrich. The ethyl(dimethylaminopropyl) carbodiimide (EDC) and N-hydroxy-succinimide ester (NHS) were acquired from Sigma-Aldrich. The ssDNA oligomers, acquired from Eurofins MWG Operon (Hunstville, AL, USA), consisted of the following sequences: (a) thiolated probe ssDNA (pDNA): SH-$(CH_2)_6$-5'-TCT GAT GTG CTT TGT TCT GGA TTT CGC AGG TCC TCA AGG GCA GAA GAG TCA CTT ATG-3', and (b) complementary target ssDNA (tDNA): 5'-CAT AAG TGA CTC TTC TGC CCT TGA GGA CCT GCG AAA TCC AGA ACA AAG CAC ATC AGA-3'. This DNA sequence is a fragment of the breast cancer gene BRCA1 (chromosome 17, band 21) in which a common mutation R1443X is encountered (exon 13, codon 1443) (Li et al. 2014), responsible for breast and ovarian cancers (Lynch et al. 2009). The gold-coated borosilicate glass chips (11×11 mm^2, 0.7 mm thick) used for sensor substrates, were obtained from Arrandee^{TM} company (Werther, Germany). The chips with a 250 nm thick Au(111) film deposited on a 4 nm thick Cr interlayer were annealed at 500 °C for 1 minute to clean and recrystallize the surface. They are referred to as the Au(111) gold electrodes (Au(111) GEs). For SERS/electrochemical measurements, polycrystalline Au disk electrodes (AuDE) with 1 mm dia., obtained from Elchema (Potsdam, NY, USA), were used. Two types of gold nanoparticles were employed in this study: 50 nm spherical gold nanoparticles (AuNPs) acquired from Sigma-Aldrich and 50 nm diameter magnetic gold-coated core-shell nanoparticles, Fe_2Ni@Au, synthesized in this work according to the procedure described elsewhere (Liu et al. 2014).

2.2. Apparatus

The Raman spectra were recorded using a Nicolet DXR Dispersive Raman Microscope and Spectrometer (Thermo Fisher Scientific, Waltham, MA, U.S.A.). Surface-enhanced Raman scattering (SERS) measurements were performed in the spectral range of 500-3500 cm^{-1} using a

stabilized 633 nm He-Ne laser with 8 mW power, focused onto a 0.7 μm diameter spot. For the analysis of spectral changes during sensor preparation and interactions with drugs, signal averaging over 5 μm long line on sample with 10 spectra averaged has been used. Voltammetric measurements were performed using a standard electrochemical setup with a potentiostat-galvanostat Model PS-205B from Elchema (Potsdam, NY, U.S.A.) and a Data Logger and Control System, Model DAQ-716v, operating under Voltscan 5.0 data acquisition and processing software (Elchema), was employed. A double-junction Ag/AgCl electrode was used as the reference electrode and a Pt wire as the counter electrode. All electrode potentials are referred vs. saturated Ag/AgCl reference electrode. Cyclic voltammetry (CV) and differential pulse voltammetry (DPV) were used for characterizing the biosensors' film permeability to redox probe ions (0.5 mM Fe^{2+}, uncomplexed).

2.3. Preparation of AuDE/CYS/rGO/AuNP/pDNA nanobiosensors

The commercial Au electrode was cleaned using a standard procedure consisting of polishing with 0.05 μm alumina powder (3 min) and scanning the potential between −0.4 and 1.7 V *vs.* SCE, in 0.5 M H_2SO_4 solution (scan rate v = 100 mVs^{-1}), until a CV characteristic for clean Au electrode was obtained. Then, Au electrode was immersed in a 15 mM CYS solution for 30 min, as illustrated in Fig. 1, and washed with deionized water. The CYS-SAM on AuDE substrates was deposited to bind the graphene oxide (GO) film. The AuDE@CYS electrode formed was subsequently immersed in a diluted GO aqueous solution (0.5 mg/mL) with carboxyl groups activated using EDC/NHS, enabling amide bonding of single layer GO sheets. Thus, a Au/CYS/GO electrode was obtained. Finally, the electrode was scanned in 0.5 M NaCl solution from 0.7 to −1.1 V at a scan rate of 50 mV s^{-1} in order to partially reduce the GO to the reduced graphene oxide (rGO) (Kubesa et al. 2014; Wang et al. 2009), thereby converting it to a Au/CYS/rGO electrode. Different types of gold nanoparticle solutions (AuNPs and Fe_2Ni@Au) were used to form a nanoparticle monolayer on the sensor surface. The synthesis of magnetic nanoparticles, Fe_2Ni@Au, was described earlier (Liu et al. 2014). Briefly, $FeSO_4.7H_2O$ and $NiCl_2$ were dissolved into 100 mL deionized water in proper molar ratio and pH was adjusted to 5.8 with NaOH. The reduction of Fe(II) and Ni(II) was carried out under N_2, using hydrazine hydrate as the reducing agent and sodium citrate and ethylene glycol as the surfactants, in an

autoclave at 120 ºC for 19 h followed by magnetic separation of Fe_2Ni NPs. Detailed X-ray, magnetic, thermogravimetric, and spectroscopic characteristics of Fe_xNi NP alloys of this preparation have been published elsewhere (Liu et al. 2014). The gold nanoparticle solutions (AuNPs, Fe_2Ni@Au, 20 µL) were spotted on Au/CYS/rGO electrode for 1 h until dried and adsorbed on the rGO layer (Ilkhani et al. 2013). After washing with distilled water, the Au/CYS/rGO/AuNPs electrode obtained was incubated with a thiolated ssDNA probe in phosphate buffer solution (pH 7.4) by dropping 20 µL of the probe solution until dried, following washing with deionized water for three times. Thus obtained nanobiosensor is branded as Au/CYS/rGO/AuNPs/pDNA (Fig. 1).

The Au(111)/HDT,OT/AuNP/pDNA sensors were synthesized by forming a HDT-SAM on Au(111), binding AuNPs, and immobilizing pDNA. The mixed SAM of HDT and OT on Au(111) substrates was to provide free sulfhydryl groups from HDT for binding AuNPs or Fe_2Ni@Au NPs. OT is playing the role of space filling and preventing HDT from flat orientation on the substrate. The details are presented in *SI*. The methods used for hybridization of tDNA with pDNA and the procedure for intercalating DOX into dsDNA are also described in *SI*.

Fig. 1.

The effect of anticancer drugs on DNA was investigated using the model chemotherapeutic drug, doxorubicin (DOX). The chemical structure of DOX is presented in Scheme 1.

Scheme 1.

3. Results and discussions

3.1. Design of DNA biosensors for drug testing

The interactions of anticancer drugs with dsDNA were investigated to assess the drug-induced modifications to DNA. The biosensors designed for this purpose were based on the SERS/electrochemical transduction and utilized covalent binding of plasmonic nanostructural

elements: spherical solid gold nanoparticles and magnetic gold-coated nanoparticles, to a self-assembled monolayer (SAM) of dithiols or a reduced graphene oxide (rGO) nanosheet basal layer on gold substrates. A widely used chemotherapeutic drug, doxorubicin (DOX), was employed as the model anti-cancer drug and the interactions of DOX with a breast cancer dsDNA duplex were investigated. For the first time, the SERS/electrochemical transduction was used to detect the intercalation of DOX molecules into the double helix of dsDNA molecules immobilized on AuNP and Fe_2Ni@Au nanoparticles captured on SAM-protected Au(111) GE and AuDE surfaces. The processes involved in nanostructured biosensors construction are illustrated in Fig. 1. The SERS nanobiosensor depicted in panel A is based on the Au(111) smooth gold surface with mixed HDT-OT SAM and captured AuNPs that are functionalized with dsDNA. In panel B, presented is the SERS/electrochemical nanobiosensor with a polycrystalline gold substrate protected with a SAM of CYS and reduced graphene oxide (rGO) with covalently attached AuNPs or Fe_2Ni@Au NPs functionalized with dsDNA.

3.2. SERS spectroscopy of DNA immobilized on Au(111)/HDT/AuNPs biosensor surface

The SERS active nanobiosensors, synthesized by modifying Au(111) GE with AuNPs, followed by incubation with pDNA probe, were characterized by SERS to verify the functionalization process. The SERS spectrum for Au(111)/HDT/AuNP/pDNA is presented in Fig. 2.

Fig. 2.

The main bands are observed at Raman shifts: 3057, 2892, 2180, 1614, 1557, 1398, 1182, 1006, and 966 cm^{-1}. Of these, the modes at 3057 and 2892 cm^{-1} are assigned to stretching vibrations of aromatic and aliphatic CH groups, respectively. Three intense bands at 1614, 1557, and 1006 cm^{-1} correspond to the immobilized ssDNA while the band at 2180 cm^{-1} originates from SAM bonding to ssDNA. Since a strong band at 1604 cm^{-1} was reported for deoxyadenosine 5'-phosphoric acid (dAMP) for 266 nm excitation (Fodor et al. 1985) and this band, shifted toward higher energies in calf thymus DNA, was reported at 1621 cm^{-1} (Lee et al. 2004), the SERS band observed for our pDNA immobilized on AuNPs at 1614 cm^{-1} can be

assigned to the adenine vibrations mode. Also, for a deoxyguanosine 5'-phosphoric acid (dGMP), a Raman bands at 1578 cm^{-1} has been observed (Fodor et al. 1985). Thus, the SERS band observed for our pDNA immobilized on AuNPs at 1557 cm^{-1} can be assigned to guanine vibrations. The weak Raman band at 1398 cm^{-1} is very close to band reported for deoxythymidine 5'-phosphoric acid (dTMP) at 1385 cm^{-1} (Lee et al. 2004). Finally, the strong Raman band at 1006 cm^{-1} corresponds to symmetric stretch vibrations of PO_2^- (Stanicová et al. 1999) and thus corresponds to all nucleotides in pDNA. The presence of these modes confirms that the pDNA probe was successfully attached to the AuNP surface.

We have also investigated the behavior of SERS biosensors with covalently attached gold-coated core-shell magnetic NPs, Fe_2Ni@Au, functionalized with single-stranded and double-stranded DNA. These specially designed and fabricated magnetic NPs exhibit superparamagnetic properties which aid in handling NP functionalization and recovery, as well as recycling for further use.

3.3. Raman mapping of sensor surface film

To evaluate the effect of AuNPs deposited on the SERS sensors, Raman mapping has been performed. In Fig. 3a, the 2D mapping for an area of 800×600 μm^2 is presented. This mapping shows a relatively even distribution of NPs on the sensor surface. The intense red areas correspond to clusters of AuNP@pDNA. The matrix of spots on the nanosensor surface where the SERS spectra were taken is shown in Fig. 3b. The spot matrix consists of a 16×12 grid, with one averaged spectrum taken for each cross point. Thus, the number of SERS spectra taken for the image in Fig. 3a was 2,210 (221 spots times 10 spectra per point for averaging). The 3D Raman mapping is presented in Fig. 3c. For the enhanced mapping, a larger number of cross points can be selected to obtain finer details and higher resolution images but it takes longer time to acquire large number of images. The minimum Raman laser spot was 0.7 μm.

Fig. 3.

3.4. SERS investigations of doxorubicin interactions with DNA using AuDE nanobiosensors with gold-coated magnetic nanoparticles Fe_2Ni@Au

SERS spectrum for the gold-coted magnetic core-shell nanoparticles, Fe_2Ni@Au, modified with pDNA and dsDNA, after hybridization with tDNA target, are presented in Fig. 4.

Fig. 4.

The high intensities of SERS peaks observed for both the ssDNA and dsDNA modifications of AuDE/CYS/rGO/Fe_2Ni@Au biosensors are likely due to the high plasmonic field magnification on the relatively small NPs. These spectra confirm that the ssDNA immobilization and hybridization with tDNA were successfully performed.

After the hybridization of the ssDNA probes with complementary tDNA target, the Raman shifts were recorded, as illustrated in Fig. 4b. It is seen that the SERS signal at 1292 cm^{-1} for pDNA covered sensor is 1.87 times higher in the presence of tDNA than in its absence which is associated with increasing number of DNA strands after duplex formation. It is also important that the spectrum structure has changed. It can be seen that the ratio of SERS peak intensities for peak at 1292 cm^{-1} to that for peak at 1542 cm^{-1} changed from 1.725 to 0.789, for pDNA alone and pDNA-tDNA duplex, respectively.

Subsequently, the DOX interactions with dsDNA immobilized on the SERS biosensor have been investigated. The obtained SERS spectra are presented in Fig. 4, curve c. It is seen that the spectrum for the sensory film has changed reflecting the DOX intercalation into the dsDNA duplex and DNA-DOX complex formation. After addition of DOX, the intensity of SERS peak at 1292 cm^{-1} increased slightly (by 12 %) but the ratio of SERS peak intensities for peak at 1292 cm^{-1} to that for peak at 1542 cm^{-1} changed from 0.789 to 1.33, for pDNA-tDNA duplex alone and after intercalation of DOX, respectively. In particular, a decrease of the Raman intensity of the main band at 1542 cm^{-1} is observed while the band intensity at 1292 cm^{-1} is increased. The latter band can be assigned to the C-O vibrations in ring A of DOX which is known to not intercalate into the DNA duplex (Beljebbar et al. 1995). These vibrations were previously observed at 1275 cm^{-1} for 514 nm excitation (Lee et al. 2004) and at 1296 cm^{-1} for 633 nm excitation (Gautier et al. 2013), at different SERS substrate geometries. The decrease of the

intensity at 1542 cm^{-1} is likely due to the decrease in hydrogen bonding to C=O groups caused by DOX intercalation. A new band, which appears after DOX intercalation at 944 cm^{-1}, can be assigned to C-C vibrations in ring A of DOX (which were encountered as ring breathing at 985 cm^{-1} in SERS measurements (Beljebbar et al. 1995) and at 990 cm^{-1} in Raman spectroscopy for DOX in solution (Gautier et al. 2013) but were only barely discernible at 912 cm^{-1} using UV resonance Raman spectroscopy (Lee et al. 2004)). The more intense peaks at 1210 and 1244 cm^{-1} due to in plane bending of hydroxyl groups at rings C and D, δ(O-H), described recently for DOX in solution in pH range 4 to 10, are not present on the spectrum (c), likely due to the intercalation of the rings into the DNA.

The SERS spectra of the DNA-DOX complex immobilized on the nanostructured surface of a biosensor are consistent with crystallographic X-ray studies (Frederick et al. 1990) indicating that rings B and C of DOX are intercalated between the guanine and adenine bases while the ring A of DOX remains outside of the duplex and the sugar ring parks in the minor groove, interacting there with base pairs neighboring the intercalation center.

The DNA-DOX complex prevents synthesis of macromolecules (Tacar et al. 2013). More importantly, DOX inhibits the enzyme topoisomerase II from relaxing dsDNA supercoils necessary for transcription (Pommier et al. 2010) and then, it prevents the dsDNA duplex from resealing after the strands are cut for replication (Tacar et al. 2013). Also, DOX induces the generation of ROS and organic free radicals. The ability of the SERS nanobiosensors to provide information about the anticancer drug interaction with DNA and its intercalation into DNA double helix is a unique feature of this type of biosensors which can be further utilized in studies of anticancer drug affinity to DNA and in new drug development.

3.5. Voltammetric characterization of SERS/electrochemical biosensors modified with DNA-functionalized AuNPs and Fe_2Ni@Au NPs

Further studies of nanobiosensors with SERS/electrochemical transduction were performed using electrochemical measurements with CV and DPV techniques. For the electrochemical investigations, the AuDE surface was modified with a reduced graphene oxide (rGO) covalently attached to CYS-SAM since this modification provides better interfacial electron transfer

conditions than the dithiol SAM resulting in less hindrance and higher effective current densities. The GO modified Au electrodes were used to attach functionalized AuNPs, followed by the immobilization of ssDNA probe and reduction of GO to rGO. The electrochemical behavior of such prepared modified Au electrodes was studied using CV and DP voltammetries with uncomplexed $Fe^{2+/3+}$ redox probe. The obtained results are shown in Fig. 5 (and in *SI*, Fig. S1).

Fig. 5.

As can be seen in Fig. 5, the redox peak currents (CV and DPV) increase and the peaks show more reversible behavior (CV) after the electrode is modified with rGO and gold-coated magnetic Fe_2Ni@Au nanoparticles. These changes result from the increased electrochemically-active electrode surface area achieved by these modifications. The film conductivity and the electron transfer improve as well. Then, after the immobilization of ssDNA, the redox peak currents decrease dramatically. The sharp decrease is due to the increased film thickness and lengthening of the diffusional path of the redox probe ions to the electrode surface. After hybridization, the current decreases even more due to the tighter probe diffusion space. The addition of DOX initiates the interaction of the drug molecules with the immobilized dsDNA which results in DOX intercalation into the DNA duplex and modification of the DNA structure, leading to the decreased DNA film structure integrity and the increased film permeability to the Fe^{2+} ion probe. This is reflected in a pronounced redox-current increase after DOX intercalation.

Similar results were obtained using different types of gold nanoparticles. The best surface covering (lowest current after ssDNA immobilization) and the best drug-DNA signal has been found for biosensors modified with Fe_2Ni@Au NPs. The increased thickness of Au shell in these NPs (not shown) has led to lower DPV signals. The experiments performed with AuNP modifications for AuNPs with 50 nm dia. and 100 nm dia. (not shown) indicate that 50 nm NPs offer better performance than that of larger NPs.

3.6. Concentration dependence of DOX intercalation into dsDNA

It is important for the drug development to determine if the drug acts in concentration-dependent manner. Therefore, the interactions of DOX, as the model chemotherapeutic drug,

with DNA immobilized on the biosensor surface have been tested using DPV for varying DOX concentration. The obtained results are presented in Fig. 6.

Fig. 6.

In this graph, the difference between the biosensor DPV currents before and after the DOX injection, Δi_p, is plotted vs. DOX concentration in the range from 0.003 to 5 mg/mL. At concentrations higher than 5 mg/mL, the signal of the biosensor leveled off. This means that for concentrations of DOX higher than 5 mg/mL, all active sites in dsDNA double helix have already been filled with DOX. Each point on the calibration plot in Fig. 6 is the average of three repetitive measurements and the standard deviation of the three measurements provides the metrics to evaluate the repeatability of the biosensor responses.

As shown in Fig. 6, the electrochemical signal of the biosensor at lower concentrations of DOX rises more steeply than that at higher concentrations of DOX, indicating that the data for the full range of DOX concentrations, from 0.003 to 5 mg/mL, cannot be fitted with a single linear regression equation. The logarithmic equation of the form: $\Delta i_p = = 2.655 \log(c_{DOX}) + 6.584$ fits the experimental data reasonably well ($R^2 = 0.994$). In this equation, Δi_p is in [μA] and c_{DOX} is in [mg/mL]. The limit of DOX detection is 0.008 mg/mL, for S/N ration 3:1 ($\sigma = 0.323$ μA, $n = 11$).

This test of the proposed biosensor demonstrates that the dose–response relationship for a chemotherapeutic drug can be assessed with high sensitivity and shows, in this particular case, that DOX acts in a concentration-dependent manner.

3.7. Reproducibility and selectivity

The reproducibility of DPV peak measurements for 1 mg/mL DOX using AuDE/CYS/rGO/Fe_2Ni@Au/dsDNA biosensor was 3.42% (Δi_p = 6.43±0.22 μA, n = 5). For SERS signals, there are many options for performing signal averaging including changing the slit width, exposition time, number of repetitive measurements, and ratiometric data treatment. The signal is highly specific depending on the vibrational mode selected. Note that no Raman tags

were used in the experiments. The SERS sensing is based on the recognition of Raman active molecular vibrations and as such it is one of the most specific sensing techniques utilized for chemical identification. The sensor developed in this work was designed for screening new drugs and their effects on DNA samples. Since this type of work requires thousands of potential drugs to be tested, the method relies on pure standard DNA molecules. To eliminate variability inherent with real biological DNA samples, well-defined synthetic DNA molecules were immobilized in the sensory film.

4. Conclusion

We have demonstrated that the nanobiosensors AuDE/CYS/rGO/Fe_2Ni@Au/dsDNA with SERS/electrochemical transduction have the capability of monitoring DNA modification or damage induced by anticancer drugs and thus have the potential for utilization in drug screening to aid in the development of new cancer therapies. We have shown for the first time that the drug intercalation into a DNA double helix can be assessed using label-less nanobiosensors with tandem SERS/electrochemical transduction. While the chemically-specific SERS signals identify the intercalation mode, the electrochemical relaxation signals provide high sensitivity enabling drug dose-efficacy evaluation. Future applications of the biosensors developed in this work may also include investigations carried out to design theranostic nanocarriers, testing of drug release dynamics, and analytical determination of drugs interacting with DNA in pharmaceutical formulations.

Therefore, the proposed sensor employs pure DNA samples embedded in the sensory film instead of external biological samples. In this way, the drug screening can be performed reliably, fast, and unambiguously. The elimination of multiple influences and focusing solely on drug interactions with DNA are here a requirement rather than a matter of choice. In the next step of the new drug development, the selected drug candidates need to be rigorously tested under different conditions on real biological samples and in exchange interactions with other drugs, etc.

Acknowledgements

This work was supported by SUNY Research Collaboration Fund (RF Project No. 1114594) and the SUNY Network of Excellence.

Appendix A. Supplementary material

Supplementary data associated with this article can be found in the online version at http://

References

Baia, L., 2012. J. Biosens. Bioelectron. 3(2), e110.

Bantz, K.C., Meyer, A.F., Wittenberg, N.J., Im, H., Kurtuluş, O., al., e., 2011. Phys. Chem. Chem. Phys. 13, 11551-11567.

Beljebbar, A., Sockalingum, G.D., Angiboust, J.F., Manfait, M., 1995. Spectrochim. Acta A 51(12), 2083-2090.

Benvidi, A., Firouzabadi, A.D., Tezerjani, M.D., Moshtaghiun, S.M., Mazloum-Ardakani, M., Ansarin, A., 2015. J Electroanal Chem 750, 57–64.

Brauhut, S.J., McIntosh, D., Vorotnikova, K., Zhou, T., Marx, K.A., 2005. Assay Drug Dev. 3, 77088.

Burgess, D.J., 2012. Nat. Rev. Cancer 12, 737.

Chikkaveeraiah, B.V., Bhirde, A.A., Morgan, N.Y., Eden, H.S., Chen, X., 2012. ACS Nano 6, 6546–6561.

Chon, H., Lee, S., Son, S.W., Oh, C.H., Choo, J., 2009. Anal. Chem. 81, 3029–3034.

Du, X.J., Tang, L.L., Chen, L., Mao, Y.P., Guo, R., Liu, X., Sun, Y., Zeng, M.S., Kang, T.B., Shao, J.Y., Lin, A.H., 2015. Sci. Rep. 5, 16664.

Eliasson, C., Lorén, A., Murty, K.V.G.K., Josefson, M., Käll, M., Abrahamsson, J., Abrahamsson, K., 2001. Spectrochim. Acta A 57(9), 1907–1915.

Feng, S., al., e., 2011. Biosens. Bioelectron. 26, 3167–3174.

Feng, S., al., e., 2013. Analyst 138, 3967–3974.

Fodor, S.P.A., Rava, R.P., Hays, T.G., Spiro, T.G., 1985. J. Am. Chem. Soc. 107, 1520-1529.

Frederick, C.A., Williams, L.D., Ughetto, G., al., e., 1990. Biochem. 29(10), 2538-2549.

Galandová, J., Ovádeková, R., Ferancová, A., J., J.L., 2009. Anal. Bioanal. Chem. 394(3), 855-861.

Gautier, J., Munnier, E., Douziech-Eyrolles, L., Paillard, A., Dubois, P., Chourpa, I., 2013. Analyst 138, 7354-7361.

Hepel, M., Stobiecka, M., 2010. Interactions of Herbicide Atrazine with DNA. Nova Science Publishers, New York.

Hepel, M., Stobiecka, M., 2011. Novel DNA-Hybridization Biosensors for Studies of Atrazine Interactions with DNA. In: Daniels, J.A. (Ed.), Adv. Environ. Res., pp. 253-298. Nova Sci. Publ., New York.

Hepel, M., Stobiecka, M., Nowicka, A., 2012a. Nanogravimetric and voltammetric DNA-biosensors for screening of herbicides and pesticides. In: Preedy, V.R., Patel, V. (Eds.), Biosensors and Environmental Health, pp. 230-255. CRC Press, Boca Raton, FL.

Hepel, M., Stobiecka, M., Peachey, J., Miller, J., 2012b. Mutation Res. 735, 1-11.

Holohan, C., Schaeybroeck, S.V., Longley, D.B., Johnston, P.G., 2013. Nat. Rev. Cancer 13, 714-726.

Huh, Y., Chung, A., Erickson, D., 2009. Microfluid. Nanofluid. 6, 285-297.

Ilkhani, H., Arvand, M., Ganjali, M.R., Marrazza, G., Mascini, M., 2013. Electroanalysis 25(2), 507-514.

Imani, R., Iglič, A., Turner, A.P.F., Tiwari, A., 2014. Electrochem. Commun. 40, 84-87.

Kubesa, O., Morrisey, K., Matthews, S., Proetta, J., Li, C., Skladal, P., Hepel, M., 2014. Mediterr. J. Chem. 3, 916-928.

Labib, M., Khan, N., Ghobadloo, S.M., Cheng, J., Pezacki, J.P., Berezovski, M.V., 2013. J. Am. Chem. Soc. 135, 3027-3038.

Lee, C.J., Kang, J.S., Kim, M.S., Lee, K.P., Lee, M.S., 2004. Bull. Korean Chem. Soc. 25, 1211-1216.

Lee, K., Drachev, V.P., Irudayaraj, J., 2011. ACS Nano 5, 2109-2117.

Li, J., Skeete, Z., Shan, S., Yan, S., Kurzatkowska, K., Zhao, W., Ngo, Q.M., Holubovska, P., Luo, J., Hepel, M., Zhong, C.J., 2015. Anal. Chem.

Li, M., Cushing, S.K., Zhang, J., Suri, S., Evans, R., Petros, W.P., Gibson, L.F., Ma, D., Liu, Y., Wu, N., 2013. ACS Nano 7, 4967–4976.

Li, Y., Yan, Y., Lei, Y., Zhao, D., Yuan, T., Zhang, D., Cheng, W., Ding, S., 2014. Colloids Surfaces B: Biointerf. 120, 15-20.

Lierop, D.V., Faulds, K., Graham, D., 2011. Anal. Chem. 83, 5817-5821.

Lim, D.K., al., e., 2011. Nat. Nanotech. 6, 452–460.

Lin, D., Pan, J., Huang, H., Chen, G., Qiu, S., Shi, H., Chen, W., Yu, Y., Feng, S., Chen, R., 2014. Sci. Rep. 4, 4751.

Liu, H., Zhang, L., Lang, X., Yamaguchi, Y., Iwasaki, H., Inouye, Y., Xue, Q., Chen, M., 2011. Sci. Rep. 1, 112.

Liu, Y., Chi, Y., Shan, S., Yin, J., Luo, J., Zhong, C.J., 2014. J. Alloys Compd. 587, 260-266.

Lu, L., Xu, L., Kang, T., Cheng, S., 2013. Appl Surf Sci 284, 258-262.

Lynch, H.T., Casey, M.J., Snyder, C.L., Bewtra, C., Lynch, J.F., Butts, M., Godwin, A.K., 2009. Mol. Oncol. 3(2), 97-137.

Miskovsky, P., Chinsky, L., Wheeler, G.V., Turpin, P.Y., 1995. J. Biomol. Struct. Dyn. 13, 547-552.

Nabiev, I.R., Morjani, H., Manfait, M., 1991. Eur. Biophys. J. 19(6), 311-316.

Nowicka, A.M., Kowalczyk, A., Stojek, Z., Hepel, M., 2010. Biophys. Chem. 146, 42-53.

Oliveira-Brett, A.M., Vivan, M., Fernandes, I.R., Piedade, J.A.P., 2002. Talanta 56(5), 959-970.

Ovádeková, R., Jantová, S., Letasiová, S., Stepánek, I., Labuda, J., 2006. Anal. Bioanal. Chem. 386(7-8), 2055-2062.

Panikkanvalappil, S.R., Mackey, M.A., El-Sayed, M.A., 2013. J. Am. Chem. Soc. 135, 4815–4821.

Pommier, Y., Leo, E., Zhang, H., Marchand, C., 2010. Chem. Biol. 17(5), 421-433.

Prescott, B., Steinmetz, W., Jr, G.T., 1984. Biopolymers 23, 235-256.

Samanta, A., Maiti, K.K., Soh, K.S., Liao, X., Vendrell, M., Dinish, U.S., Yun, S.W., Bhuvaneswari, R., Kim, H., Rautela, S., Chung, J., Olivo, M., Chang, Y.T., 2011. Angew. Chem., Int. Ed. 50, 6089–6092.

Sha, M.Y., al., e., 2008. J. Am. Chem. Soc. 130, 17214–17215.

Sha, M.Y., Xu, H.X., Natan, M.J., Cromer, R., 2008. J. Am. Chem. Soc. 130, 17214.

Stanicová, J., Fabriciová, G., Chinsky, L., Sutiak, V., Miskovsky, P., 1999. J. Mol. Struct. 478, 129-138.

Tabakman, S.M., Chen, Z., Casalongue, H.S., Wang, H.L., Dai, H.J., 2011. Small 7, 499-505.

Tacar, O., Sriamornsak, P., Dass, C.R., 2013. J. Pharm. Pharmacol. 65(2), 157-170.

Tang, W., Zhang, M., Li, W., Zeng, X., 2014. Talanta 127, 262-268.

Tokonami, S., Yamamoto, Y., Shiigi, H., Nagaoka, T., 2012. Anal. Chim. Acta 716, 76-91.

Tripp, R.A., Dluhy, R.A., Zhao, Y., 2008. Nano Today 3, 31-37.

Wang, G., al., e., 2011a. Anal. Chem. 83, 2554–2561.

Wang, X., al., e., 2011b. Cancer Res. 71, 1526–1532.

Wang, Z., Zhou, X., Zhang, J., Boey, F., Zhang, H., 2009. The Journal of Physical Chemistry C 113(32), 14071-14075.

Wei, W., Ni, Q., Pu, Y., Yin, L., Liu, S., 2014a. Journal of Electroanalytical Chemistry 714–715(0), 25-29.

Wei, W., Ni, Q., Pu, Y., Yin, L., Liu, S., 2014b. J Electroanal Chem 714-715, 25-29.

Xiong, H., Chen, Y., Zhang, X., Gu, H., Wang, S., 2013. Sens Actuators, B Chem 181, 85-91.

Yang, Y., Yin, X., Sheng, L., Xu, S., Dong, L., Liu, L., 2015. Sci. Rep. 5, 12850.

Ye, S., Yang, Y., Xiao, J., Zhang, S., 2012. Chem. Commun. 48, 8535–8537.

Zhang, G.J., Huang, M.J., Ang, J.J., Liu, E.T., Desai, K.V., 2011a. Biosens. Bioelectron. 26(7), 3233-3239.

Zhang, Q., Dai, P., Yang, Z., 2011b. Microchim. Acta 173(3-4), 347-352.

Zhang, Y., Liu, H., Hu, N., 2012. Bioelectrochemistry 86, 67-71.

Zhang, Z.L., Wen, Y.Q., Ma, Y., Luo, J., Jiang, L., Song, Y.L., 2011c. Chem. Commun. 47, 7407-4709.

Scheme and Figure captions

Scheme 1. Structure of anticancer drug doxorubicin (DOX).

Fig. 1. Construction of SERS/electrochemical nanobiosensors for testing of anti-cancer drug interactions with DNA: (A) SERS biosensor with Au(111) substrate coated with a self-assembled monolayer (SAM) of hexanedithiol (HDT) + octanethiol (OT) with covalently attached gold nanoparticles (AuNPs) or magnetic Fe_2Ni@Au NPs functionalized with ssDNA probe; (B) SERS/electrochemical nanobiosensor with gold disk electrode (AuDE) substrate protected with a SAM of CYS and reduced graphene oxide (rGO) with covalently attached AuNPs or Fe_2Ni@Au NPs functionalized with dsDNA.

Fig. 2. SERS spectrum for a pDNA-modified Au(111)/DODT/AuNPs surface; AuNP size: 50 nm dia.

Fig. 3. . Raman mapping of thiolated ssDNA-modified AuNPs covalently attached to a Au(111) gold electrode surface with HDT SAM: (A) SERS image of a Au(111)/HDT/AuNPs/pDNA biosensor surface with color-coded SERS intensity at 1292 cm^{-1} (from 33 (blue) to 700 (red)); (B) imaging spots: 16×12 spots (800×600 nm^2) shown on an optical image; (C) 3D map of SERS intensity. Size of AuNPs: 50 nm dia.

Fig. 4. SERS spectra for a AuDE nanobiosensor with Fe_2Ni@Au nanoparticles: (a) modified with a probe ssDNA, (b) after hybridization of the probe ssDNA with complementary tDNA strand to form dsDNA duplex, (c) after incubation of dsDNA with chemotherapeutic drug, doxorubicin (DOX). Inset: details of high frequency peak.

Fig. 5. (A) Cyclic voltammograms for a AuDE electrode in 0.5 mM uncomplexed Fe^{2+} redox probe in 50 mM PBS: (a) bare AuDE electrode, (b) after modification with rGO, (c) after modification with magnetic core-shell Fe_2Ni@Au NPs, (d) after modification of magnetic NPs with ssDNA probe, (e) after hybridization of ssDNA probe on magnetic NPs with complementary target tDNA, (f) after interaction of the immobilized dsDNA with DOX; scan rate v = 100 mV/s. (B) Differential pulse voltammograms for: (a) rGO-coated AuDE@CYS electrode, (b) after modification with magnetic core-shell Fe_2Ni@Au NPs, (c) after modification

of magnetic NPs with ssDNA probe, (d) after hybridization of DNA probe on magnetic NPs with complementary ssDNA target, (e) after interaction of the immobilized dsDNA with DOX.

Fig. 6. (A) Dependence of DPV peak current increase Δi_p on DOX concentration c_{DOX} for AuDE with covalently bound dsDNA-modified Fe_2Ni@Au nanoparticles. (B) Linear semi-logarithmic calibration curve, $R^2 = 0.994$, $\sigma = 0.323$ μA, LOD = 0.008 mg/mL (3σ).

TOC Graphics Abstract

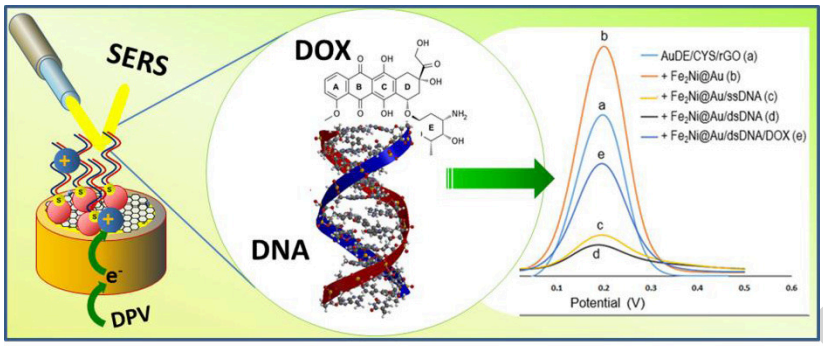

Fig. 0 TOC.

Highlights

- Novel nanobiosensors with SERS/electrochemical transduction for chemotherapeutic drug screening have been developed.
- Superparamagnetic Fe_2Ni@Au nanoparticles covalently bound to partially-reduced graphene oxide provide plasmonic field enhancement.
- Intercalation of anticancer drug doxorubicin (DOX) into a breast cancer DNA has been detected.
- Proposed biosensors offer chemical identification capability and high sensitivity with limit of detection LOD = 8 μg/mL for DOX (S/N = 3σ).

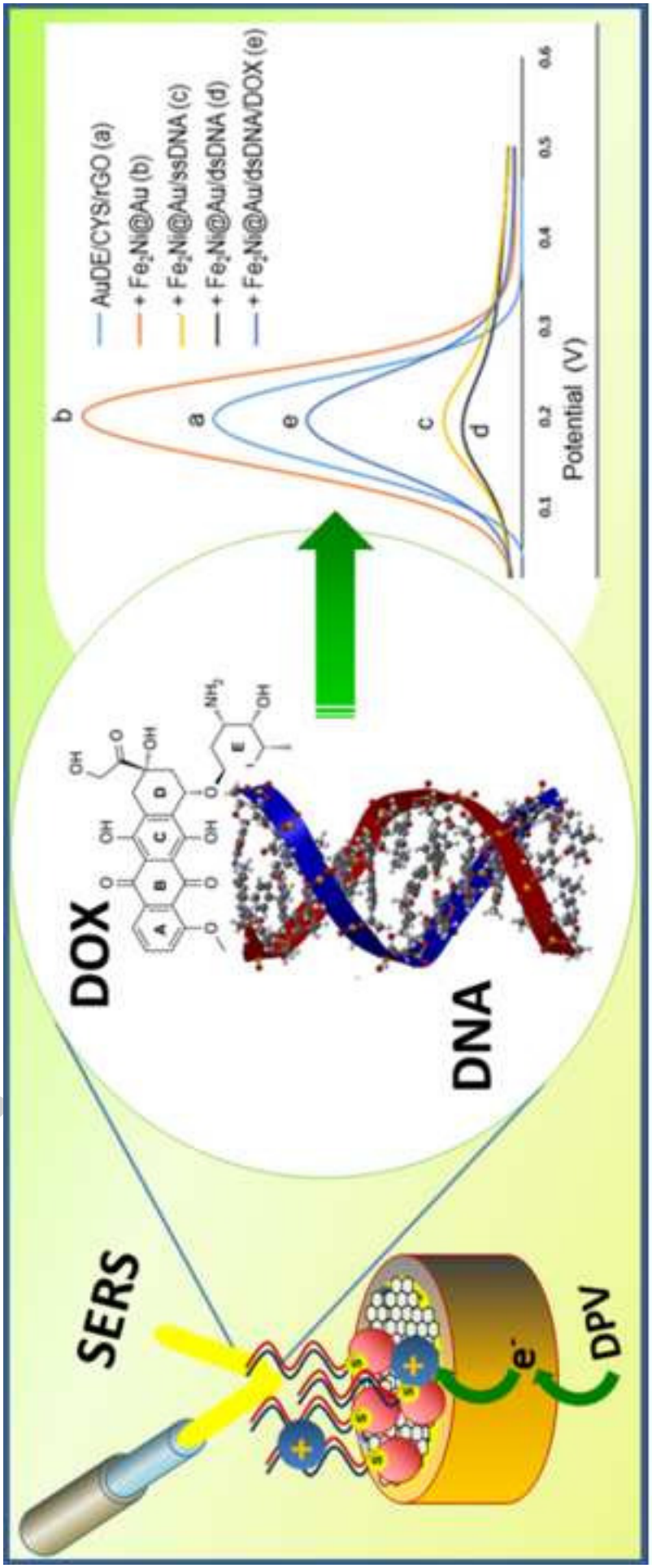
AuDE/CYS/rGO (a)
+ Fe3Ni@Au (b)
+ Fe3Ni@Au/ssDNA (c)
+ Fe3Ni@Au/dsDNA (d)
+ Fe3Ni@Au/dsDNA/DOX (e)
b
a
e
c
d
0.1
0.2
0.3
0.4
0.5
0.6
Potential (V)
DOX
DNA
SERS
e-
DPV

Figure(s)

Figure(s)

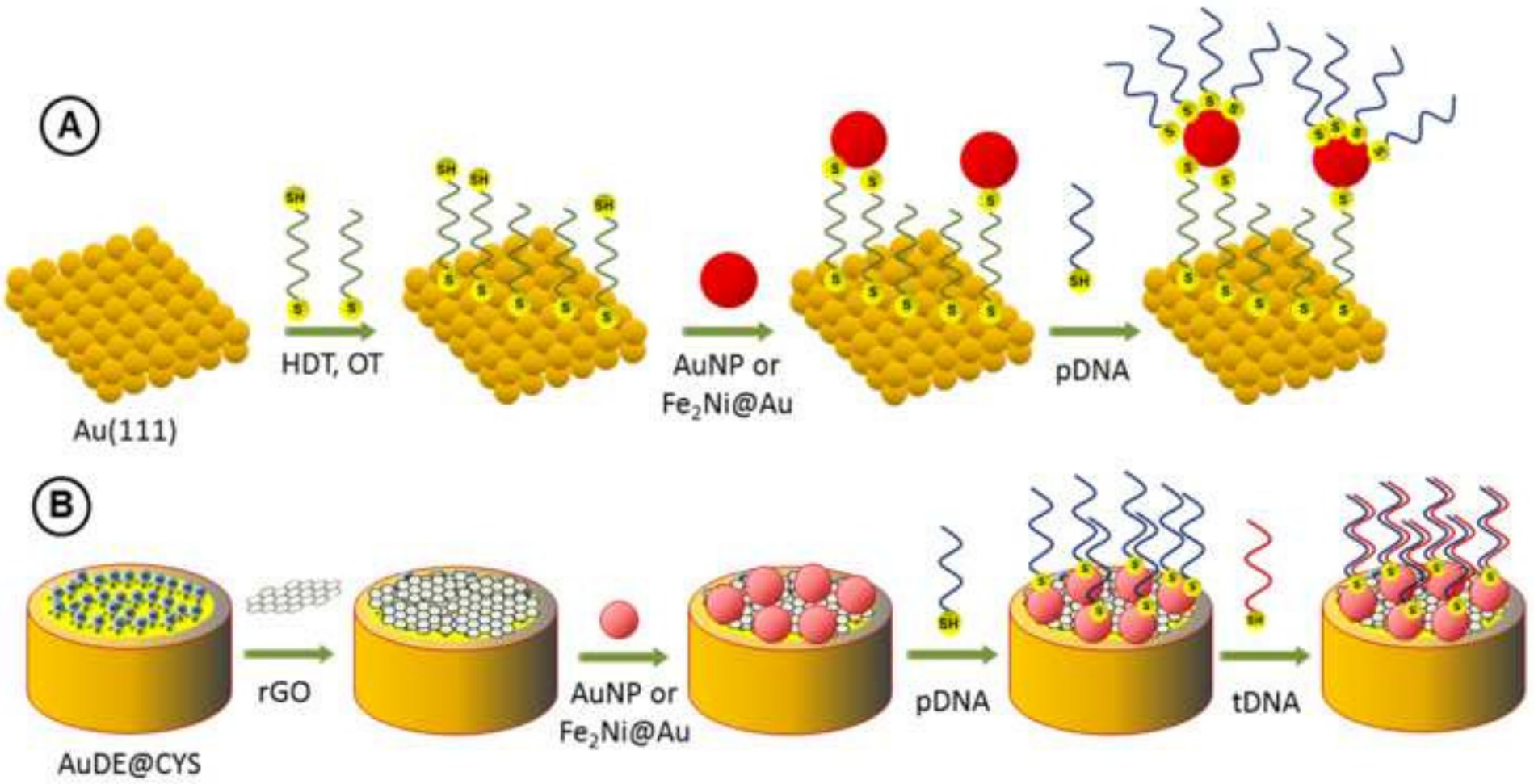

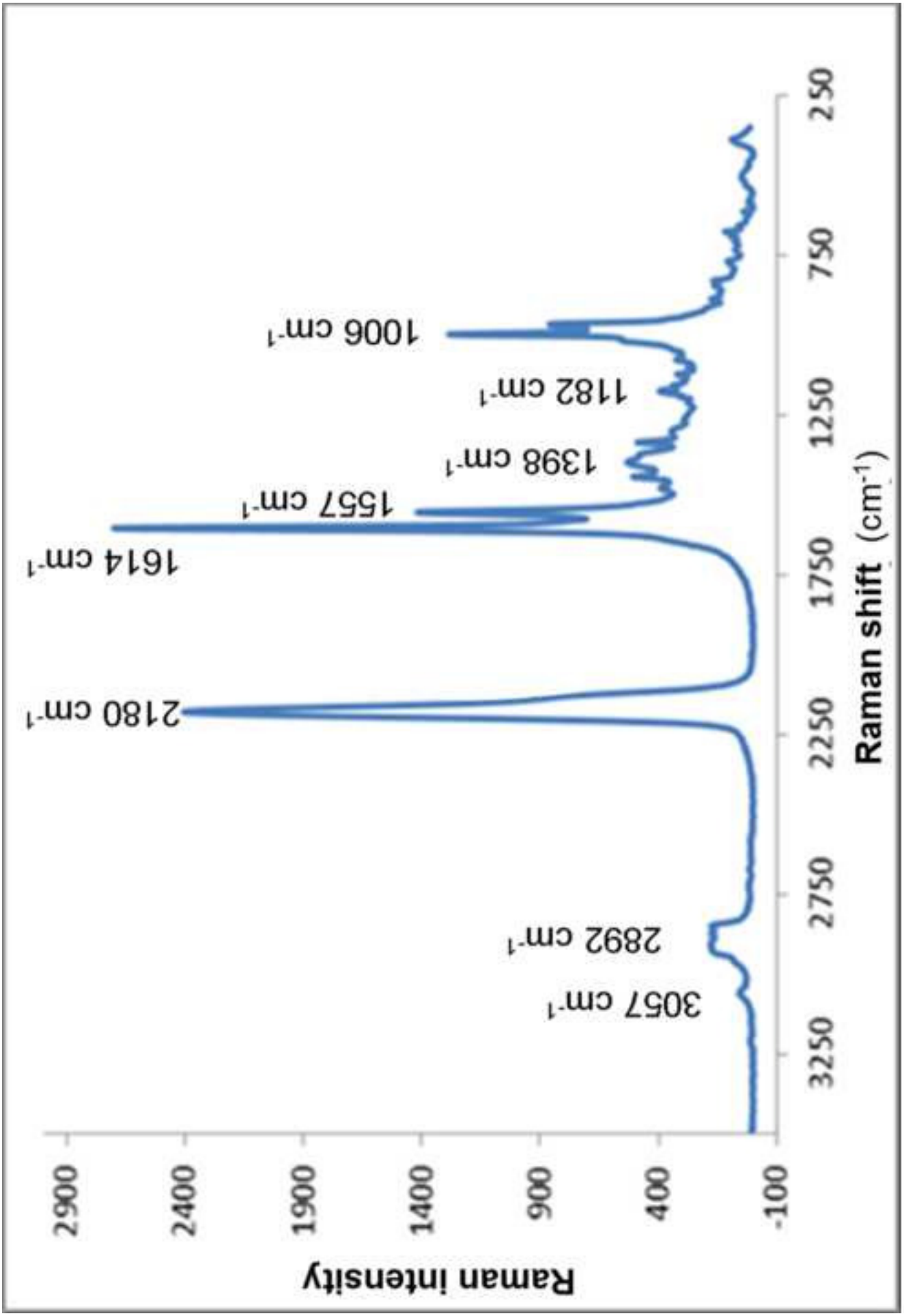
Raman intensity
2900
2400
1900
1400
900
400
-100
Raman shift (cm-1)
3250
2750
2250
1750
1250
750
250
3057 cm-1
2892 cm-1
2180 cm-1
1614 cm-1
1557 cm-1
1398 cm-1
1182 cm-1
1006 cm-1

Figure(s)

Figure(s)

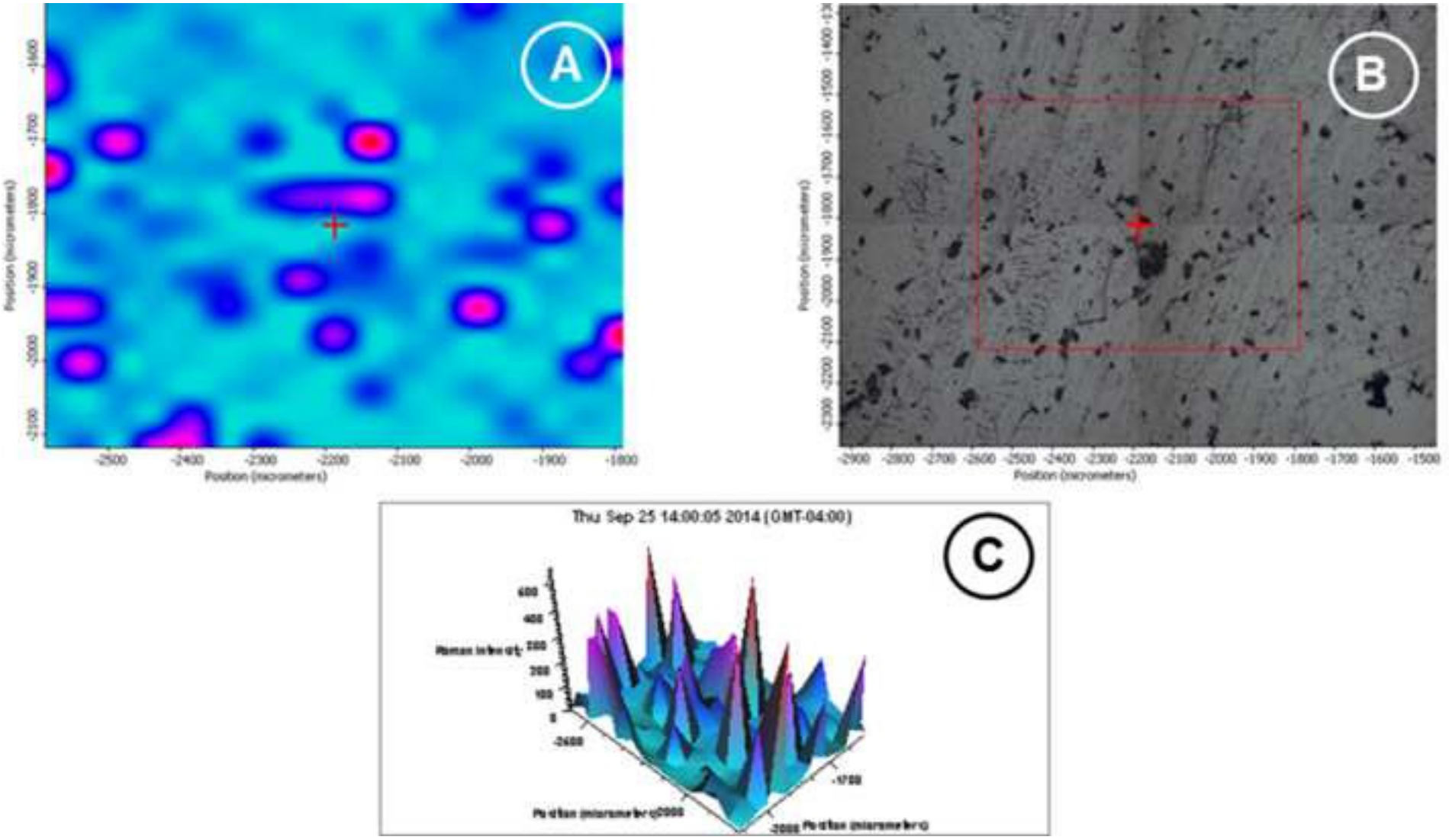

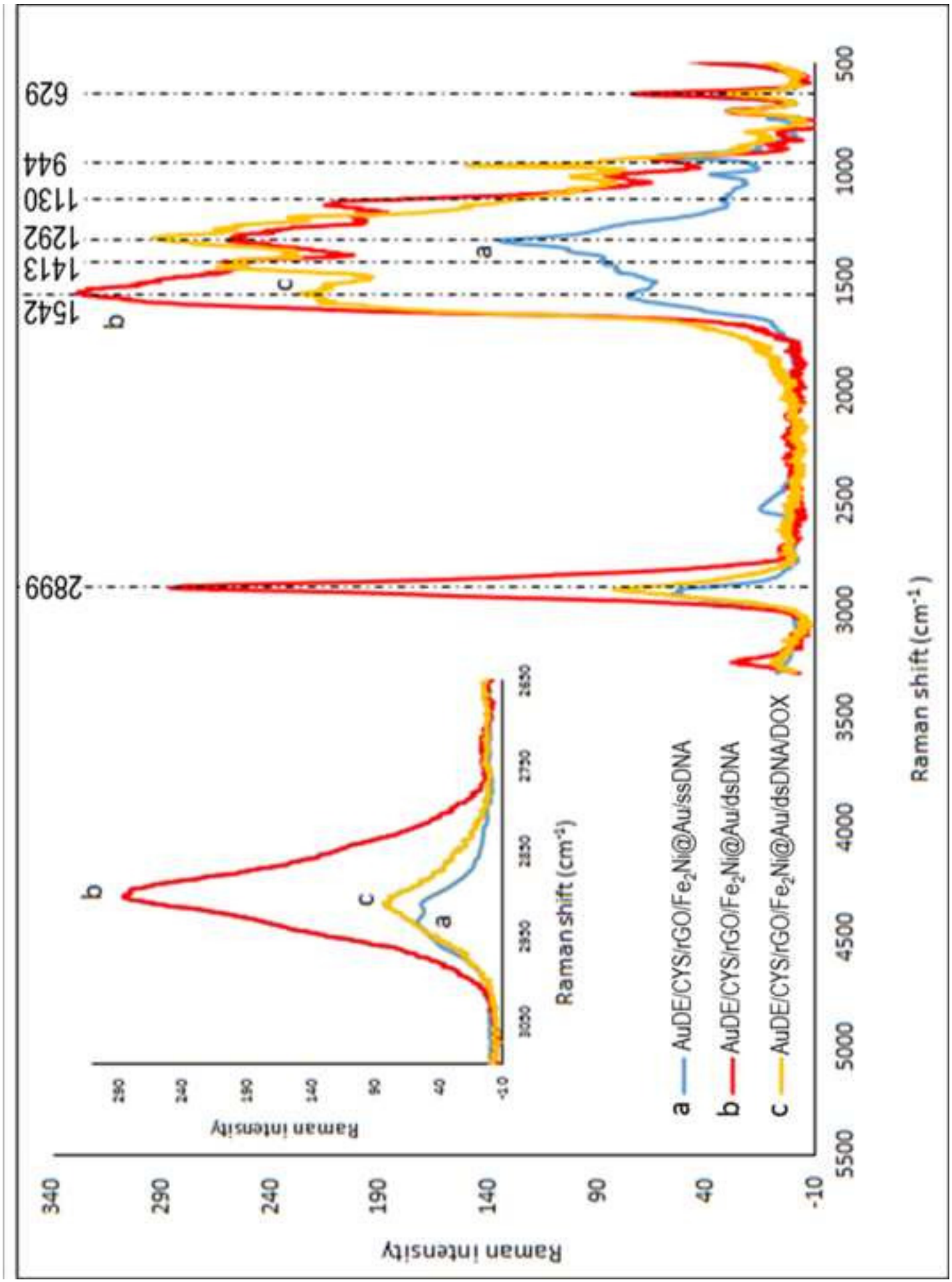
Raman intensity
Raman shift (cm-1)
a AuDE/CYS/rGO/Fe2Ni@Au/ssDNA
b AuDE/CYS/rGO/Fe2Ni@Au/dsDNA
c AuDE/CYS/rGO/Fe2Ni@Au/dsDNA/DOX
629
944
1130
1292
1413
1542
2899
a
b
c

Figure(s)

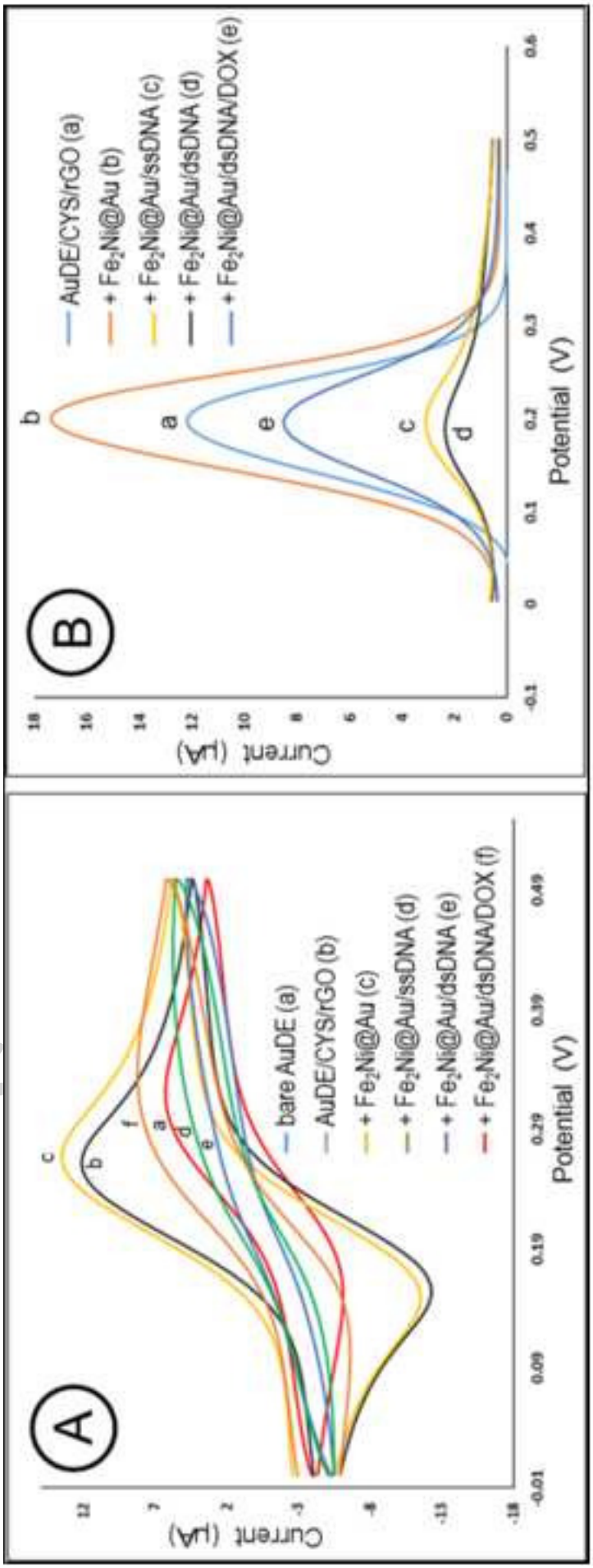
A
bare AuDE (a)
AuDE/CYS/rGO (b)
+ Fe2Ni@Au (c)
+ Fe2Ni@Au/ssDNA (d)
+ Fe2Ni@Au/dsDNA (e)
+ Fe2Ni@Au/dsDNA/DOX (f)
Current (μA)
Potential (V)
B
AuDE/CYS/rGO (a)
+ Fe2Ni@Au (b)
+ Fe2Ni@Au/ssDNA (c)
+ Fe2Ni@Au/dsDNA (d)
+ Fe2Ni@Au/dsDNA/DOX (e)
Current (μA)
Potential (V)

Figure(s)

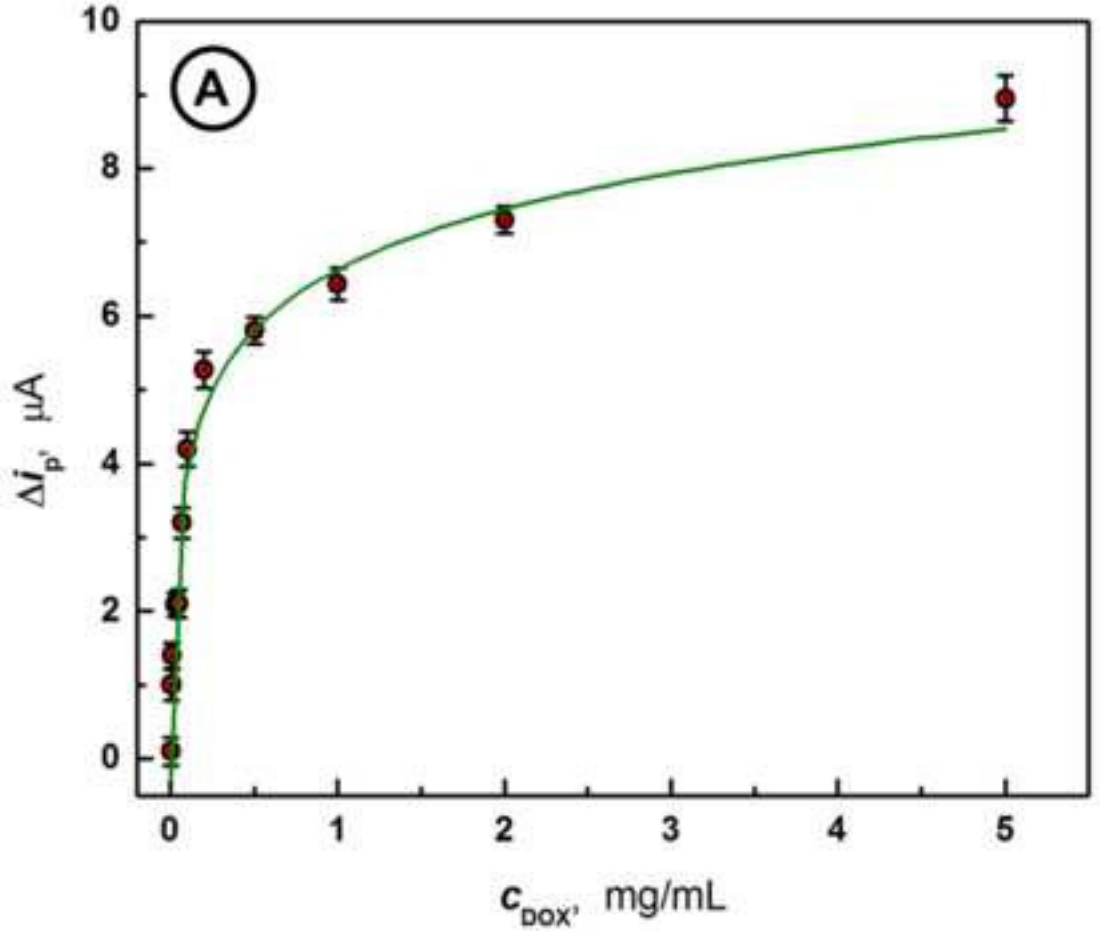

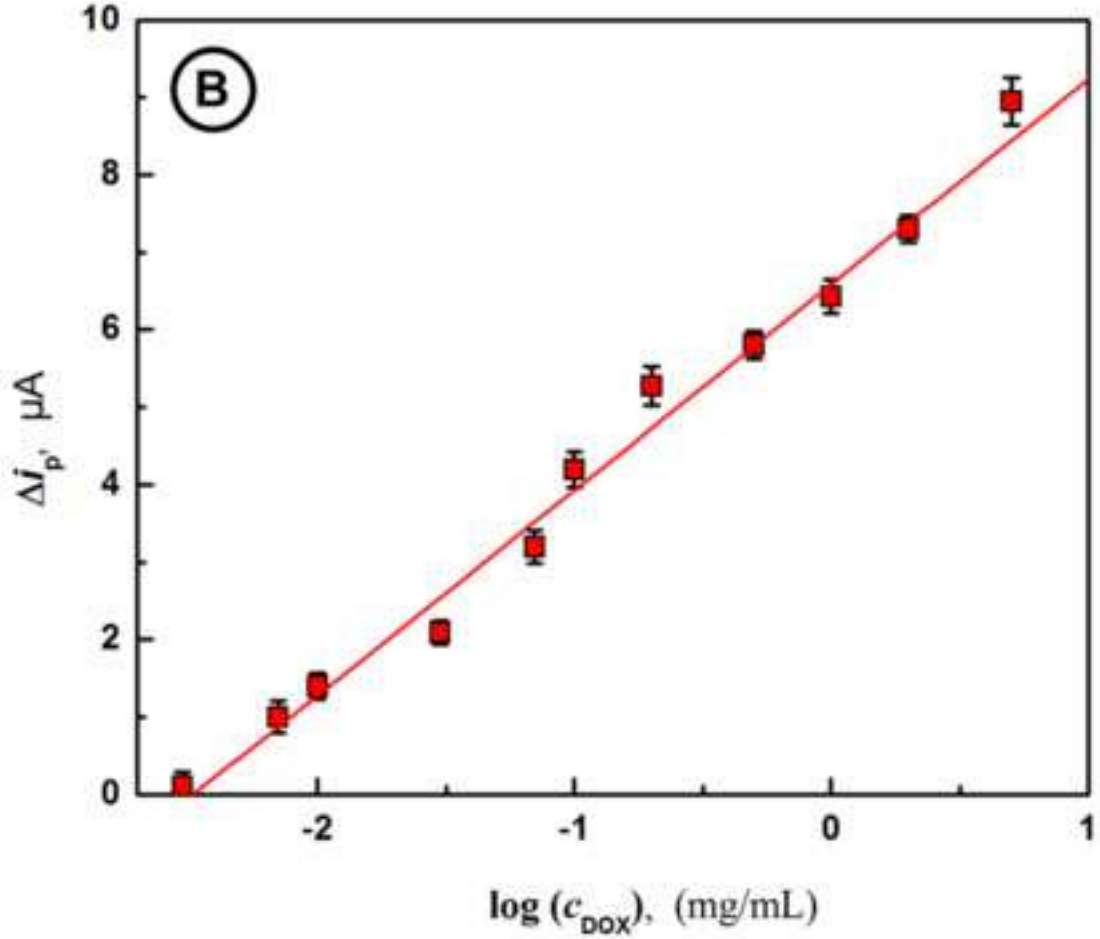

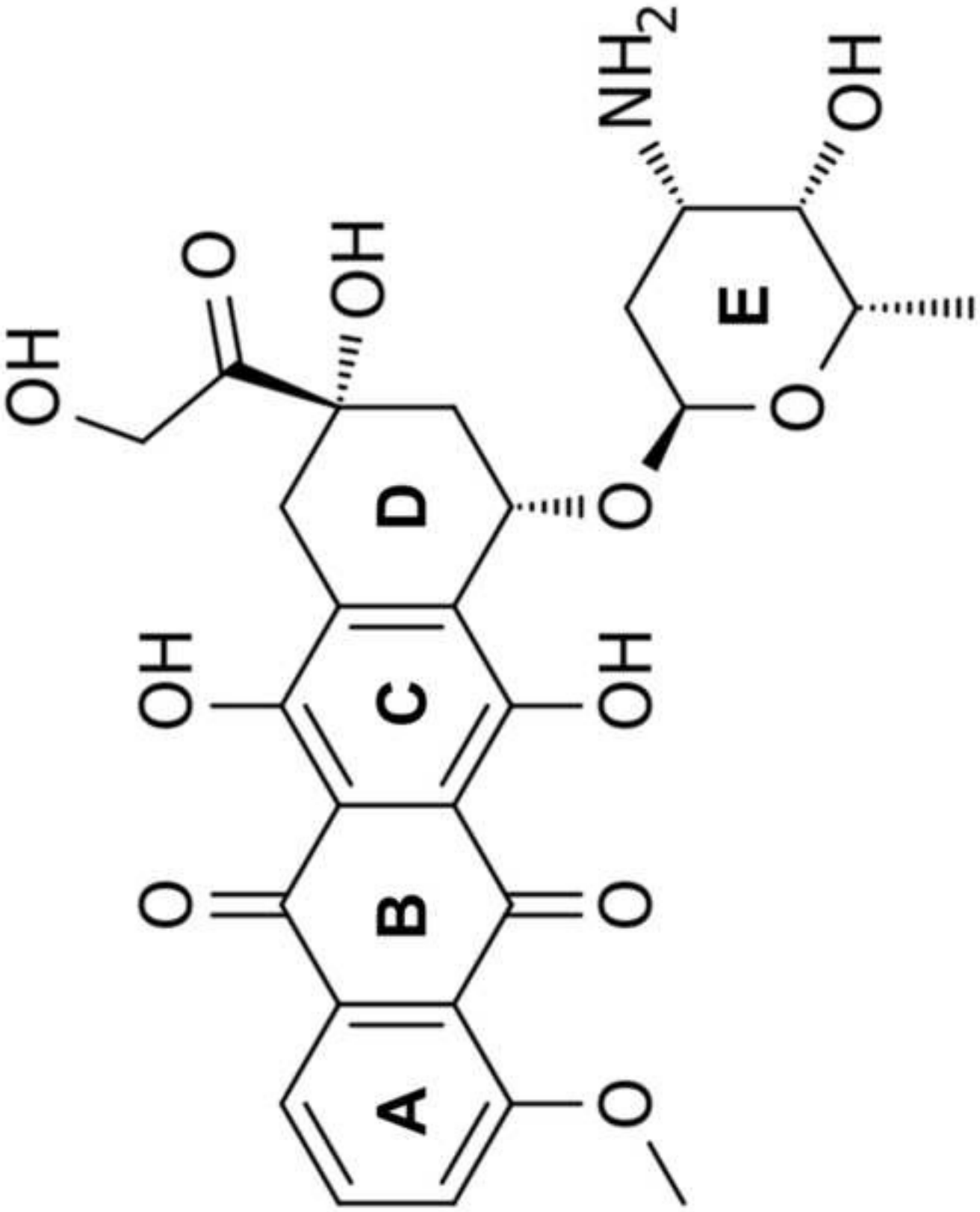

Figure(s)